ECS Transactions, 68 (1) 1509-1516 (2015)
10.1149/06801.1509ecst ©The Electrochemical Society

The Effect of Mn Co-doping on the Electrochemical Properties of $Gd_{0.2}Ce_{0.8}O_{1.9-\delta}$/Pt Model-composite Electrodes

P. Velicsanyi[a], M. Gerstl[a,b], A. Nenning[a], H. Hutter[a], J. Fleig[a], A.K. Opitz[a,b]

[a] Vienna University of Technology, Institute of Chemical Technologies and Analytics Getreidemarkt 9/164 Vienna, 1060, Austria
[b] Christian Doppler Laboratory for Interfaces in Metal-Supported Electrochemical Energy Converters, Getreidemarkt 9/164-EC Vienna, 1060, Austria

Model-type thin films of Gd doped and Gd/Mn co-doped ceria were investigated by means of impedance spectroscopy in a humid H_2 atmosphere. A novel measurement technique for microelectrodes with interdigitating Pt current collectors was employed. This method allows a separation of the different elementary processes contributing to the electrode impedance. After annealing at 650°C in humid H_2 atmosphere, an increase in catalytic activity of Gd/Mn co-doped ceria was observed.

Introduction

Owing to their remarkable catalytic activity, ceria (CeO_2) and ceria-based oxides have been attracting the attention of material science. Moreover, they have been under investigation in the recent years as anodes of SOFCs (solid oxide fuel cells) because they seem to lower the overpotential losses for the anode reaction and, being coking-resistant and sulphur-tolerant, they could realise a more flexible operation of SOFCs on hydrocarbon fuels (1-4). Electrode compositions that may lead to beneficial properties include, for example, Mn, Gd or Sm doped ceria (5-7).

In this work, gadolinium doped ceria (GDC) and manganese/gadolinium co-doped ceria (MnGDC) thin film electrodes were studied by electrochemical impedance spectroscopy, scanning electron microscopy, X-ray diffraction and time of flight secondary ion mass spectrometry. For impedance spectroscopy a special setup of thin film ceria electrodes with Pt current collectors allowed the simultaneous measurement of a range of electrochemical parameters such as surface electrocatalytic activity, ionic and electronic conductivity and chemical capacitance. These properties are compared between GDC and Mn co-doped GDC.

Experimental

YSZ (9.5 %mol Y_2O_3) single crystalline substrates with a polished side parallel to the (100) plane were purchased from Crystec, Germany. Targets of $Gd_{0.2}Ce_{0.8}O_{1.9-\delta}$ (GDC) and $Mn_{0.1}Gd_{0.18}Ce_{0.72}O_{1.9-\delta}$ (MnGDC) were prepared for PLD (pulsed laser deposition). GDC was a commercially available powder (Treibacher Industrie AG, Austria). MnGDC was synthesised from the GDC powder and $MnCO_3$ (99.9%, Sigma-Aldrich Co.): both powders were ground in a mortar and annealed at 1400°C. The powders were then cold

isostatically pressed to pellets, and sintered at 1550°C for 2.5 hours. X-ray diffraction was done in Bragg-Brentano geometry, with an X'Pert Powder PANalytical diffractometer.

Thin layers of GDC and MnGDC were prepared on YSZ by PLD at 650°C substrate temperature, controlled by a pyrometer, in a pure oxygen atmosphere at 4×10^{-2} mbar. The deposition time was chosen such to reach a film thickness of 200 nm. Pt current collectors (100 nm) with a Ti adhesion layer (5 nm) were prepared prior to ceria deposition using a magnetron sputtering machine (MCS 020, BAL-TEC AG, Germany). Microstructuring of the current collectors and the cerium oxide layers was done by photolithography and subsequent Ar ion beam etching.

For impedance measurements the thin film sample was placed on a heater (Linkam, UK) in an atmosphere of 2.5% H_2 and about 2.5% H_2O in an Ar carrier gas and contacted using gold coated steel tips. Impedance spectra were recorded using a Novocontrol Alpha AK High Resolution Impedance Analyzer with POT/GAL 30 V/2 A interface in the frequency range of 1 MHz to 10 mHz with an ac voltage of 10 mV RMS.

Results and Discussion

X-ray Diffraction

In Figure 1 XRD patterns of the macroscopic GDC and MnGDC targets are plotted. The measurements showed no second phases for GDC, while MnGDC exhibited some minor unidentifiable reflexes. The latter result hints at the possibility of Mn rich second phases.

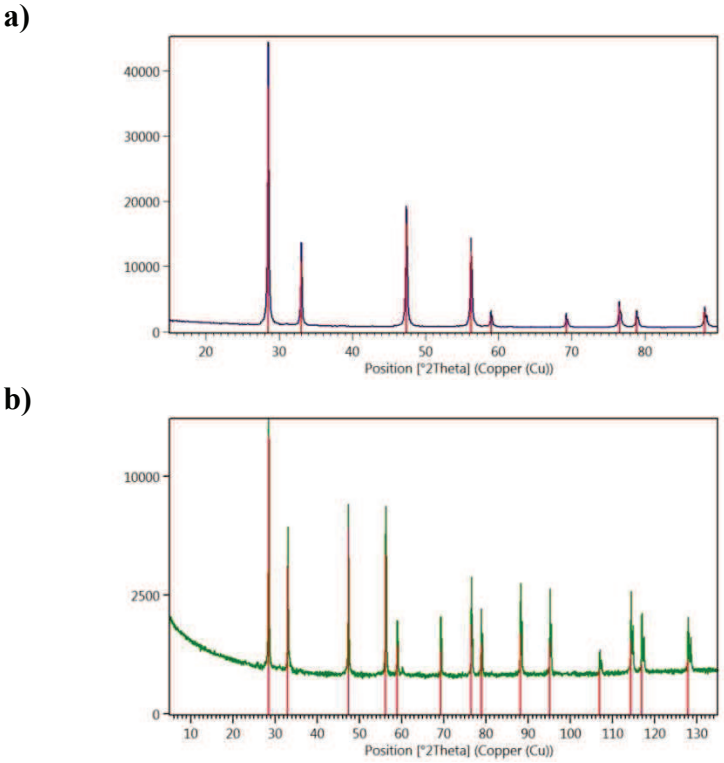

Figure 1. XRD patterns of the a) $Gd_{0.2}Ce_{0.8}O_{1.9-\delta}$ and b) $Mn_{0.1}Gd_{0.18}Ce_{0.72}O_{1.9-\delta}$ PLD targets. The red lines indicate the reference pattern of the cubic ceria structure.

Time of Flight Secondary Ion Mass Spectrometry (ToF-SIMS)

As the MnGDC target showed minor reflexes not attributable to the cerium oxide structure, the question arises, whether the thin films produced by PLD contain a homogenous distribution of Mn. To verify this, ToF-SIMS measurements were performed on exemplary films. In Figure 2a) the mass signal for Mn is shown. The comparison between the MnGDC and GDC thin film shows that a strong Mn signal is present in MnGDC, while no such feature is visible for the manganese free ceria.

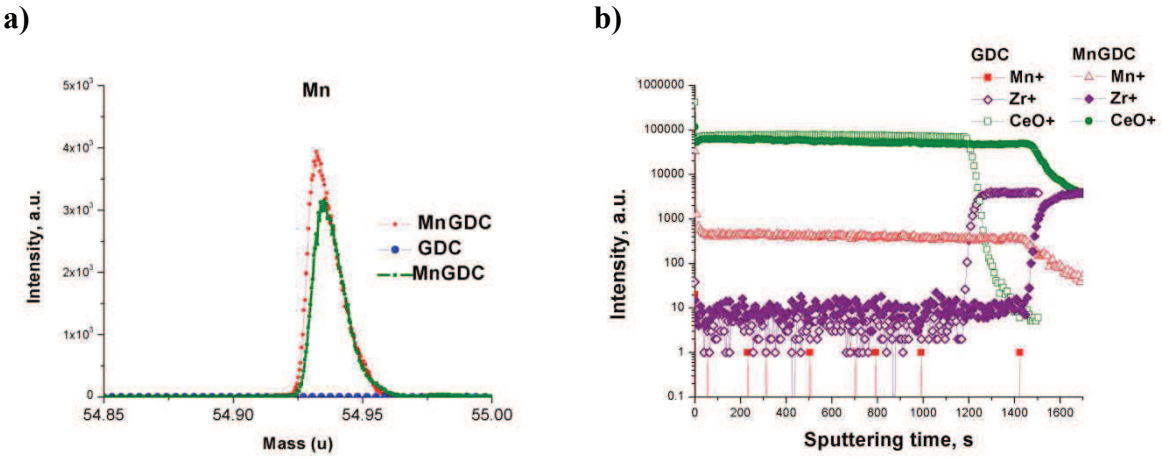

Figure 2. a) Mass signal for Mn recorded on MnGDC and GDC thin films. The Mn signal on MnGDC was measured on two positions. b) Secondary ion depth profile of GDC and MnGDC thin films on a YSZ single crystal. The sputtering time correlates linearly with depth.

The depth profile in Figure 2b) shows that Mn is homogenously distributed throughout the MnGDC thin film, while no Mn is present in the GDC sample. The first few data points taken near the surface may be interpreted as Mn enrichment and Ce depletion. However, since the Ce depletion is also present in the undoped GDC sample, a SIMS artifact appears to be the most likely interpretation.

Impedance Spectroscopy

Electrode Geometry. A special electrode design using two interdigitated current collectors beneath the GDC microelectrode in combination with a macroscopic counter electrode was used. This setup allowed two different measurement modes, called “in-plane” and “electrochemical” mode. In the first case the signal is applied between the two comb-shaped current collectors. In the second case both current collectors are short-circuited and the signal is applied versus a macroscopic counter electrode, see Figure 3. The counter electrode consists of larger stripes of GDC thin film with buried current collector. Since the size of the counter electrode is at least 100 times larger than a microelectrode its reversibility can safely be assumed.

The combination of both resulting impedance spectra – in-plane and electrochemical one – allows the simultaneous determination of electronic conductivity, ionic conductivity, area specific surface resistance and the chemical capacitance. A detailed discussion of the theoretical background of this novel method and the transmission line models used to fit the measured data can be found in Ref. (8).

Figure 4 shows the impedance spectra of one and the same electrode in both in-plane and electrochemical mode along with the fit. The excellent agreement validates the method for the further investigation.

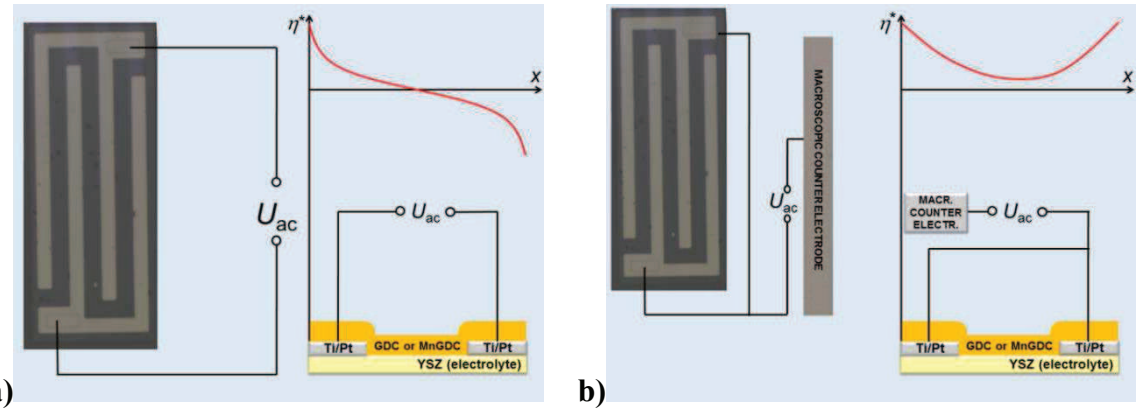

Figure 3. Sketches of a) in-plane and b) electrochemical measurement mode. The upper right graph in a) and b) shows the polarization potential distribution between two neighboring fingers (lower right graph) for each mode. The micrograph on the left side in a) and b) has a finger spacing of 25 µm and a finger width of 15µm.

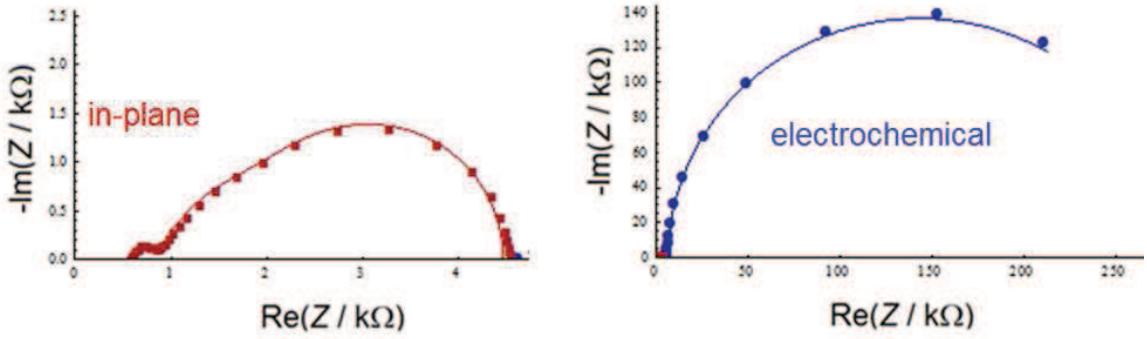

Figure 4. Examples for measured impedance spectra in in-plane and electrochemical mode for a 200nm thick MnGDC sample with buried Ti/Pt current collector at 700°C set temperature (~ 630°C real temperature). The finger spacing was 11.7 µm, finger width 15 µm and the measurements were taken in an atmosphere of 2.5% H_2 and about 2.5% H_2O in an Ar carrier gas. The symbols are the measured data points and the lines represent the fit curves.

Temperature Measurement. Due to the asymmetric heating the set temperature differs from the actual temperature of the measured electrodes. To mitigate this issue a surface temperature was calculated from the YSZ spreading resistance taken from the high frequency intercepts of the impedance spectra when measuring in electrochemical mode. If the sample thickness is much bigger than the diameter of a circular microelectrode, the ohmic drop of the YSZ electrolyte R_{YSZ} is given by (9):

$$R_{YSZ} = (2 \times \sigma_{ion,YSZ} \times d_{ME})^{-1} \quad [1]$$

In eq. 1 $\sigma_{ion,YSZ}$ is the ionic conductivity of YSZ and d_{ME} the diameter of a circular microelectrode. The spreading resistance of the rectangular electrodes used here was found to be virtually equal to that of 300 µm circular electrodes. Since the temperature

dependence of the YSZ single crystal is known (10), the electrode temperature can be approximated.

Long Term Stability. In order to detect any time-dependent variations a longer measurement was carried out at 630°C, by collecting spectra every five minutes. The electronic and ionic resistances of MnGDC did not continually change over the observed time period. However, the area specific surface resistance showed a steep decrease in the first few hours, followed by a plateau region and a slower increase afterwards, see Figure 5. Therefore, all subsequent measurements on MnGDC were performed after keeping the sample a few hours at 630°C to reach the plateau region.

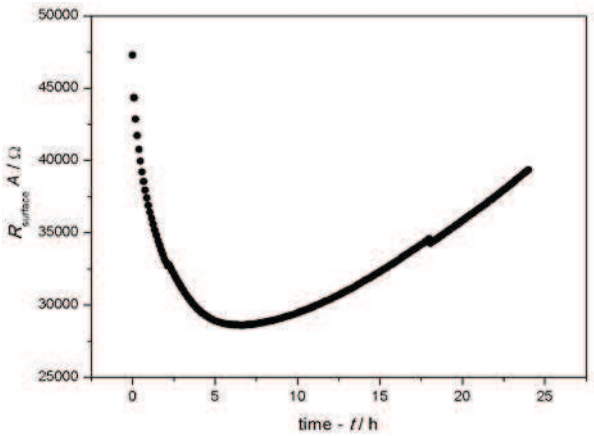

Figure 5. Change in the surface resistance of a 200 nm thick MnGDC sample at 700°C set temperature (~630°C real temperature) in an atmosphere of 2.5% H_2 and about 2.5% H_2O in an Ar carrier gas.

Activation Energies. To gather the activation energy of the various processes Arrhenius type measurements were carried out at different temperatures between 400°C and 700°C set temperature. GDC and MnGDC show very similar characteristics, however, the area specific surface resistance, plotted in Figure 6a), is about half an order of magnitude lower for MnGDC. This may be explained by a different surface chemistry, see SEM results below.

The electronic conductivity and the chemical capacitance of MnGDC shown in Figure 6b) and c) respectively are virtually undistinguishable from GDC at higher temperatures, but both are marginally lower at lower temperatures. The electronic conductivity σ_{eon} of GDC is given by

$$\sigma_{eon} = e \times u_{eon} \times [Ce^{3+}]. \quad [2]$$

with e being the elementary charge, u_{eon} the electronic mobility and $[Ce^{3+}]$ the concentration of reduced ceria, which is equal to the concentration of electronic charge carriers (11). The specific chemical capacitance C_{chem} relates to the $[Ce^{3+}]$ according to

$$C_{chem} = e^2 \times [Ce^{3+}] \times (kT)^{-1} \quad [3]$$

with k being the Boltzmann constant and T the absolute temperature (11). The temperature dependence of the electronic mobility is calculated using:

$$u_{eon} = u_{eon,0} \times (T)^{-1} \times \exp(-E_a \times (kT)^{-1}) \quad [4]$$

where E_a is the activation energy of the polaron hopping process (12, 13). Using eqs. 2-4 and knowledge of the electronic conductivity and the chemical capacitance, one can calculate the electronic mobility, which is plotted in Figure 6d). While the activation energy for the electronic mobility in GDC of about 0.5 eV is a realistic value for a polaron hopping process, the activation energy of 0.9 eV found for MnGDC is too high to be explained that way. While conclusive data is lacking, we suppose that electron trapping centres formed by the presence of Mn may play a role here.

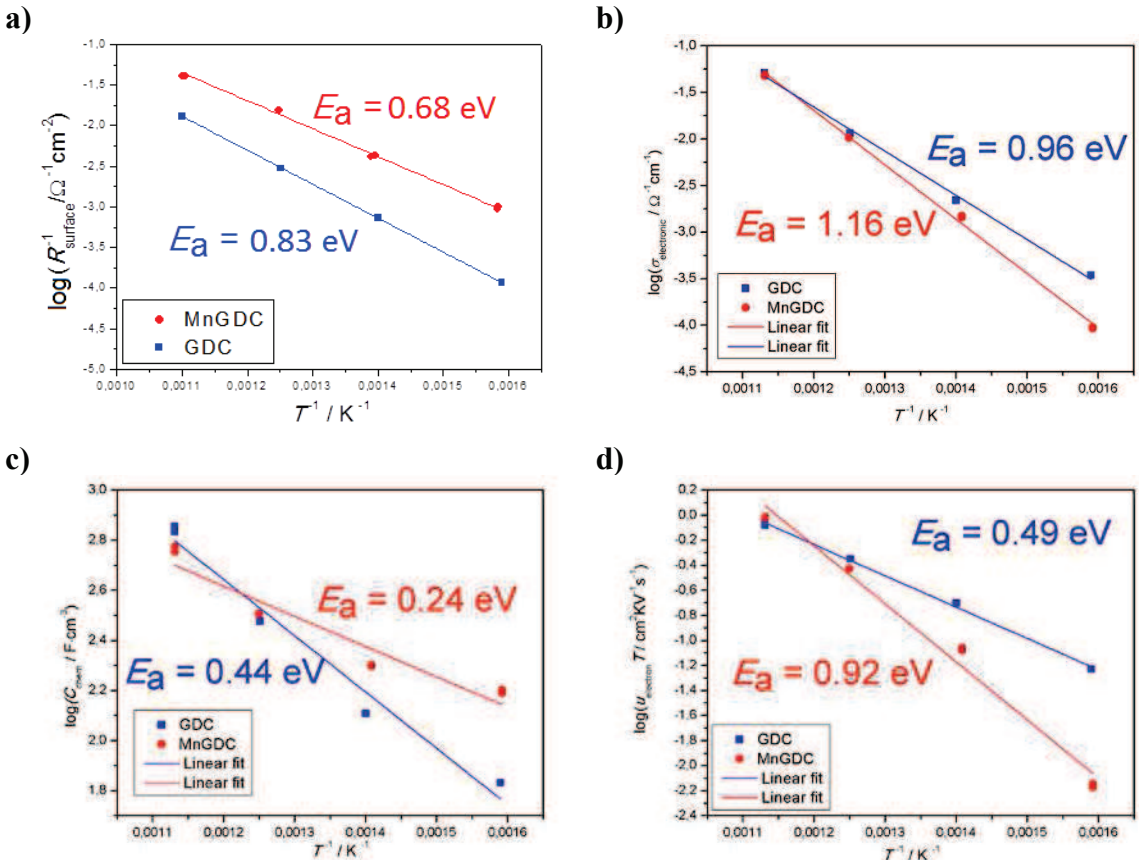

Figure 6. a) Area specific surface resistance, b) electronic conductivity, c) chemical capacitance and d) for GDC and MnGDC. Arrhenius plots between 40°C and 700°C set temperatures (~630°C real temperature) in an atmosphere of 2.5% H_2 and about 2.5% H_2O in an Ar carrier gas.

In Table I, the mean calculated activation energies for electronic and ionic conductivity, as well as the surface reaction are summarized along with their respective values at 700°C set temperature.

TABLE I. Electrochemical properties of GDC and MnGDC

Property	E_a GDC [eV]	E_a MnGDC [eV]	Value at 632°C GDC	Value at 632°C MnGDC
Electronic conductivity	0.96	1.16	0.15 S/cm	0.17 S/cm
Ionic conductivity	1.06	0.98	0.05 S/cm	0.03 S/cm
Surface reaction resistance	0.68	0.83	49 Ωcm²	22 Ωcm²

Scanning Electron Microscopy

GDC and MnGDC SEM micrographs taken after PLD and after a heat treatment of over 20h at 700°C in wet hydrogen are compared in Figure 7 and Figure 8. The freshly deposited thin films are flat, without any visible grains. After the heat treatment some coarsening in the GDC sample is observed, while on the surface of the MnGDC thin film segregations are formed. The latter might explain the higher surface catalytic activity found in the impedance spectroscopy study, because the bulk properties do not differ much for GDC and MnGDC while the surface exchange becomes much better for MnGDC. An unambiguous identification of the chemical composition and crystallographic phase of the segregations was not possible within the present study.

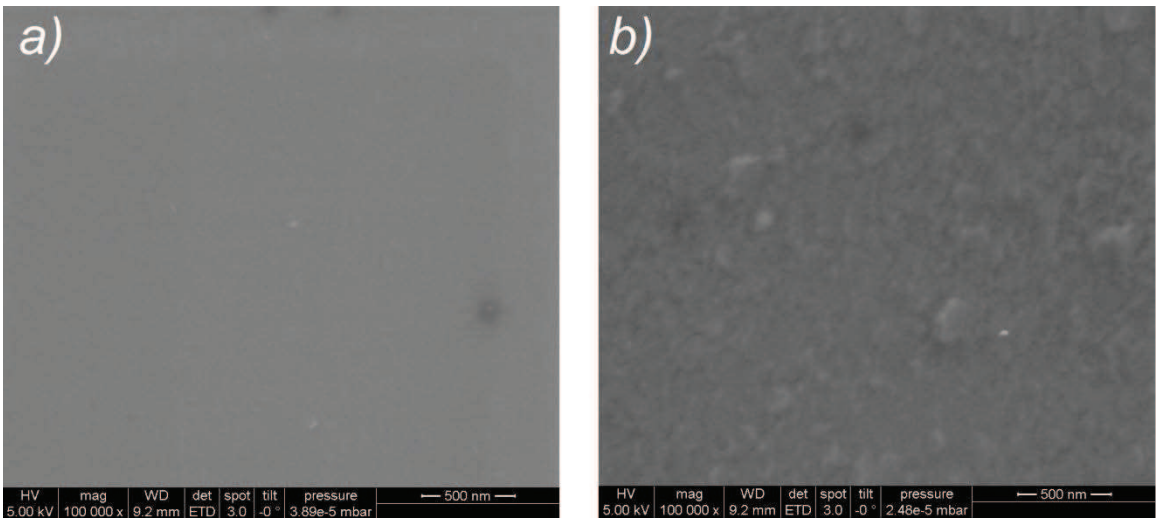

Figure 7. SEM top-views of 200 nm GDC deposited on YSZ, a) after PLD, b) after heating to 700°C for about 20 hours in an atmosphere of 2.5% H_2 and about 2.5% H_2O in an Ar carrier gas.

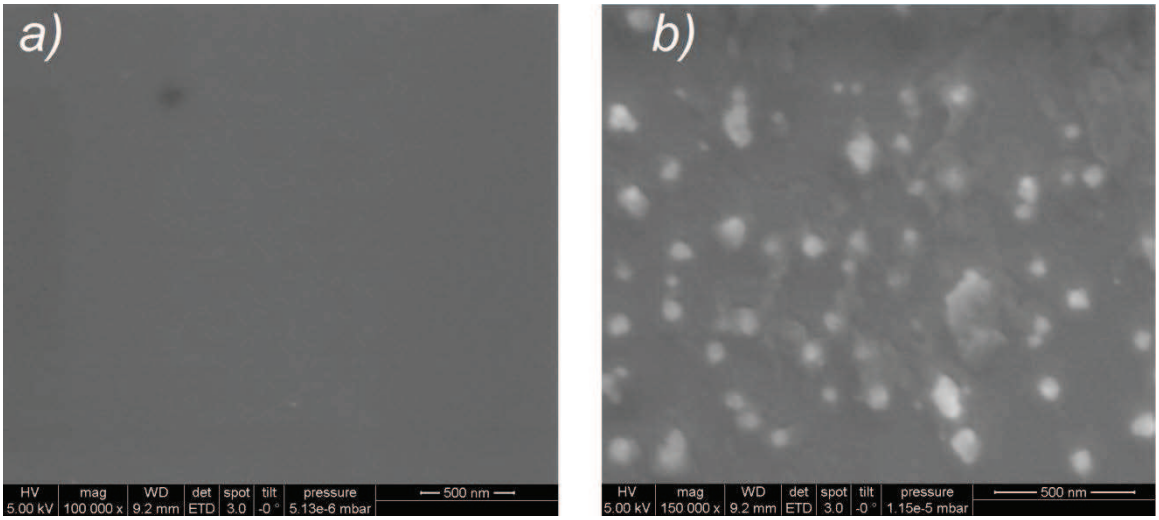

Figure 8. SEM top-views of 200 nm MnGDC deposited on YSZ, a) after PLD, b) after heating to 700°C for about 26 hours in an atmosphere of 2.5% H_2 and about 2.5% H_2O in an Ar carrier gas.

Conclusions

Thin films of $Gd_{0.2}Ce_{0.8}O_{1.9-\delta}$ and $Mn_{0.1}Gd_{0.18}Ce_{0.72}O_{1.9-\delta}$ were prepared by PLD and characterised using electrochemical impedance spectroscopy, TOF-SIMS and SEM. The thin films of MnGDC contained a homogenous Mn concentration, but showed exsolutions after tempering at 700°C for over 20 hours. The nature of this exsolutions is unclear, but it is highly likely a Mn rich phase.

Impedance spectroscopy was performed on thin film ceria microelectrodes with special Ti/Pt current collectors between 400°C and 700°C. This setup allowed the simultaneous measurement of the ionic and electronic conductivity, the surface resistance and the chemical capacitance. After a few hours at 700°C, the surface resistance was found to be lower by a factor of two for MnGDC compared to GDC, possibly connected to the surface exsolutions. However, this improvement starts to degrade after a longer heat treatment at 700°C. A slightly lower electronic conductivity and chemical capacitance in MnGDC was found at lower temperatures.

Acknowledgements

The financial support by the Austrian Federal Ministry of Science, Research and Economy, the National Foundation for Research, Technology and Development is gratefully acknowledged. This work was financially supported by the Austrian Science Fund (FWF) through grants F45-09 (SFB FOXSI) and W1243.

References

1. W. C. Chueh, Y. Hao, W. Jung and S. M. Haile, *Nature Materials*, **11**, 155 (2012).
2. W. C. Chueh, W. Lai and S. M. Haile, *Solid State Ionics*, **179**, 1036 (2008).
3. E. P. Murray, T. Tsai and S. A. Barnett, *Nature*, **400**, 649 (1999).
4. C. J. Zhang, Y. Yu, M. E. Grass, C. Dejoie, W. C. Ding, K. Gaskell, N. Jabeen, Y. P. Hong, A. Shayorskiy, H. Bluhrn, W. X. Li, G. S. Jackson, Z. Hussain, Z. Liu and B. W. Eichhorn, *J Am Chem Soc*, **135**, 11572 (2013).
5. G. Q. Cai, R. Z. Liu, C. H. Zhao, J. L. Li, S. R. Wang and T. L. Wen, *J Solid State Electr*, **15**, 147 (2011).
6. N. Kim, B. H. Kim and D. Lee, *J Power Sources*, **90**, 139 (2000).
7. T. S. Zhang, L. B. Kong, Z. Q. Zeng, H. T. Huang, P. Hing, Z. T. Xia and J. Kilner, *J Solid State Electr*, **7**, 348 (2003).
8. A. Nenning, A. K. Opitz, T. M. Huber and J. Fleig, *Phys Chem Chem Phys*, **16**, 22321 (2014).
9. J. Fleig, F. S. Baumann, V. Brichzin, H. R. Kim, J. Jamnik, G. Cristiani, H. U. Habermeier and J. Maier, *Fuel Cells*, **6**, 284 (2006).
10. A. K. Opitz and J. Fleig, *Solid State Ionics*, **181**, 684 (2010).
11. J. Jamnik and J. Maier, *Phys. Chem. Chem. Phys*, **3**, 1668 (2001).
12. L. Friedman and T. Holstein, *Ann Phys-New York*, **21**, 494 (1963).
13. T. Holstein, *Ann Phys-New York*, **8**, 343 (1959).